Records of Natural Products

Open Access
This article is licensed under CC-BY-NC-ND 4.0

www.acgpubs.org
ORIGINAL ARTICLE

Analysis of blood components and the mechanism of anti-pharyngitis and gut microbiota regulation in *Ardisia crenata* and its relatives

Zhonghui Nie[1,2#], Sha Liu[2,3#], Faming Wu[2], Chao Deng[2], Nana Tang[2], Xinyue Ke[2], Bo Huang[4], Xiaoshuang Wang[2*] and Ju Ye[1*]

[1]Department of Pharmacy, Zunyi Medical and Pharmacy College, Zunyi Medical University, Zunyi, 563000, China
[2]Zunyi Medical University, Guizhou Key Laboratory of Modern Traditional Chinese Medicine Creation, Zunyi, 563000, China
[3]Guizhou Key Laboratory of Modern Traditional Chinese Medicine Creation, Zunyi, 563000, China
[4]Chengdu Kelun Pharmaceutical Trade Co., Ltd., Chengdu, 611130, China

Cite This: *Rec. Nat. Prod.* 2027, 21(2), e26073975

Read Online

Abstract: This study comprehensively integrated network pharmacology, molecular docking, and gut microbiota analysis to explore the anti-pharyngitis targets and pathways of *Ardisia crenata* Sims (ZSG), *Ardisia crenata* Sims var.bicolor (Walk) (HLS) and *Ardisiacrispa* (Thunb.) (BLJ), and to investigate their underlying mechanisms. PPI networks and "herb-component-target-disease" networks were constructed, followed by GO and KEGG enrichment analysis. Molecular docking demonstrated strong binding affinity between the active components and the core targets. Additionally, changes in gut microbiota and endogenous metabolites in rats were analyzed by combining 16S rDNA high-throughput sequencing and untargeted metabolomics. The results revealed that the central targets are SRC, TNF, PIK3CA, STAT3, JAK2. KEGG analysis highlighted notable involvement of the PI3K/AKT, Rap1, Ras, Estrogen signaling pathways. Moreover, all three herbs were found to modulate the gut microbiota to some extent, contributing to the alleviation of microbial dysbiosis. In conclusion, ZSG, HLS and BLJ exert anti-pharyngitis effects through multi-target and multi-pathway mechanisms.

Keywords: *Ardisia crenata* Sims, anti-pharyngitis, network pharmacology, molecular docking

1 Introduction

Pharyngitis is a diffuse inflammatory condition affecting the pharyngeal mucosa, submucosal tissues, and underlying lymphoid structures (Hai et al., 2022). Driven by environmental factors such as air pollution and climate change, the incidence of pharyngitis has reached 20–50%, reflecting a growing disease burden. The clinical classification of pharyngitis primarily distinguishes between acute and chronic types (Zhang et al., 2022). Acute pharyngitis (AP) is a common upper respiratory tract infection marked by acute, non-specific inflammation, typically resulting from viral or bacterial infection, or chemical irritation (Zhao et al., 2025). At present, the clinical treatment of acute pharyngitis mainly focuses on the use of glucocorticoids, antibiotics and non-steroidal anti-inflammatory drugs (NSAIDs) (Zhaoyan et al., 2023). Chronic pharyngitis is a throat disease involving diffuse inflammation of the pharyngeal mucosa, submucosa and pharyngeal lymphoid tissue, with a high incidence rate, accounting for 10%–20% of throat diseases. According to epidemiological data, at least 20% of adults worldwide suffer from chronic pharyngitis (Wenxi & Jie, 2025). Currently, well-known international treatment methods include lozenges, laser and cryotherapy, and antibiotics (Wenxi & Jie, 2025). The Chinese Medical Association of Traditional Chinese Medicine has proposed and issued the Guidelines for the Diagnosis and Treatment of Common Diseases in Traditional Chinese Medicine Otorhinolaryngology, which provides the diagnosis, syndrome differentiation and treatment of acute pharyngitis for reference in traditional Chinese medicine treatment. Kaihoujian Spray is a Chinese patent medicine mainly used for treating sore throat, dry and bitter mouth, swollen and painful gums, oral ulcers and other symptoms caused by heat accumulation in the lung and stomach, with good therapeutic effect (Feifei & Jianlin, 2024). Its main ingredients are ZSG, *Euchresta japonica*, Periostracum

*Corresponding Authors: Xiaoshuang Wang.
Email: m18314484252@163.com; Ju Ye.
Email: yeju8145@163.com
#Contributing to the article equally

Received: July 08, 2026
Revised: August 27, 2026
Accepted: September 07, 2026
Published: November 06, 2026

Copyright © 2026. Published by ACG Publications.

Cicadae and menthol. ZSG can eliminate phlegm, promote diuresis and clear the throat; *Euchresta japonica* and menthol can reduce swelling, soothe the throat, clear away heat and toxic materials; Periostracum Cicadae can soothe the throat, improve voice, dispel wind and heat. Modern pharmacology believes that it has antipyretic, analgesic, antiviral and anti-inflammatory effects (Changzhi, 2020). ZSG, a commonly used Miao medicine in Guizhou, is made from the dried roots and rhizomes of ZSG, HLS C. Y. Wu et C. Chen and BLJ of the Myrsinaceae family. It has the effects of detoxifying and reducing swelling, promoting blood circulation and relieving pain, dispelling wind and dampness, and is often used to treat sore throat, tonsillitis, heart and stomach qi pain and other diseases (Fulin et al., 2025). In recent years, with the deepening of research, the chemical components and pharmacological effects of ZSG have gradually been revealed, and related proprietary medicines developed from it (such as "Kaihoujian Spray", a large variety of Guizhou ethnic proprietary medicines (Fulin et al., 2025)). The ZSG included in the Quality Standards for Chinese Medicinal Materials and Ethnic Medicinal Materials of Guizhou Province includes three origins: ZSG, BLJ and HLS, and the medicinal material used in the prescription of Kaihoujian Spray is ZSG (Jin-He et al., 2022). ZSG is the dried root of ZSG of the Myrsinaceae family, which is recorded in Guizhou Herbal Medicine. It is described as pungent, slightly bitter and astringent, and neutral in nature, with the effects of clearing heat, soothing the throat and promoting blood circulation, having a good therapeutic effect on pharyngitis and enjoying the reputation of a good medicine for laryngeal diseases (Wei et al., 2022). ZSG is included in the Chinese Pharmacopoeia (2020 edition), with bergenin content not less than 1.5%. It has a slightly bitter and pungent taste, a neutral nature, and belongs to the lung and stomach meridians. It mainly contains coumarins, saponins, flavonoids, volatile oils, cyclodepsipeptides, phenols, carbohydrates and other chemical components, and has pharmacological effects such as anti-inflammation, anti-tumor, anti-oxidation, hypoglycemia, liver protection, anti-fertility, cough suppression and nerve protection (Qunli et al., 2024). HLS belongs to the genus Ardisia of the Myrsinaceae family. It has a bitter and pungent taste, a cool nature, and has the effects of clearing away heat and toxic materials, and relieving pain. It contains chemical components such as triterpenoids, coumarins and phenols, and has biological activities such as anti-tumor, anti-bacterial and anti-inflammatory (Hongbo et al., 2024). BLJ is a plant of the genus Ardisia in the Myrsinaceae family. It has the effects of clearing heat, soothing the throat, promoting blood circulation, detoxifying, reducing swelling, relieving pain, and relaxing tendons and activating collaterals, and is mainly used to treat sore throat, tonsillitis, nephritis edema, and traumatic rheumatism. At the same time, modern pharmacological studies have shown that BLJ also has antibacterial, anti-inflammatory, anti-tumor and anti-oxidation effects. At present, there are few studies on the chemical components of BLJ, and only a small number of triterpenoids, flavonoids and organic acids have been reported (Rui-Hang et al., 2022). Previous studies have found that all three medicines have anti-pharyngitis effects, but their specific components and mechanisms of action are still unclear (Peng et al., 2025). Compared with the traditional single-target research method, network pharmacology and molecular docking can comprehensively reveal the interaction between compounds and disease-related targets from a systematic level, and more efficiently screen core targets and key pathways, thereby exploring the mechanism of action more deeply (Linglian & Zhigang). This article intends to predict the anti-pharyngitis pathways and targets of ZSG, HLS and BLJ, and also explore the research on the impact of these drugs on intestinal flora, which will open up prospects for future research on the clinical and pharmacological effects of ZSG, HLS and BLJ Future research still needs to continue to verify through experiments and conduct in-depth exploration on various mechanisms and pharmacological effects of the drugs.

2 Materials and Methods

2.1 Materials

Thirty-six SPF-grade male SD rats (185 ± 21 g) were provided by the Laboratory Animal Center of Zunyi Medical University (Production License No.: SCXK (Qian) 2021-0002). The animals were housed in the Laboratory Animal Facility of Zunyi Medical College, and the animal experiments complied with the requirements approved by the Laboratory Animal Ethics Committee of Zunyi Medical University (Approval No.: 56210202240601).

Voucher specimens were deposited at the Herbarium of Zunyi Medical University under the accession numbers ZSG-20231001, HLS-20231002, and BLJ-20231003. The plant materials were air-dried, ground into a coarse powder (40-mesh), and stored in airtight containers at room temperature in the dark until extraction.

HPLC-grade methanol, acetonitrile, and water were purchased from Fisher Chemical (Fair Lawn, NJ, USA). LC-MS grade formic acid and acetic acid were obtained from Merck (Darmstadt, Germany). LC-MS grade 2-propanol was purchased from Merck. The internal standard 2-chloro-L-phenylalanine (purity ≥98%) was obtained from Adamas-beta (Shanghai, China). Ammonia water (25–28%) and sodium chloride (analytical grade) were purchased from Sinopharm Chemical Reagent Co., Ltd. (Shanghai, China). Diethyl ether (anesthetic grade) was obtained from Shanghai Aladdin Biochemical Technology Co., Ltd. (Shanghai, China). All other reagents were of analytical grade and used without further purification.

The FastPure Stool DNA Isolation Kit was purchased from Majorbio Bio-Pharm Technology Co., Ltd. (Shanghai, China).

2.2 Methods

2.2.1 Acquisition of Components Entering the Blood

2.2.1.1 Preparation of the Aqueous Extract of the Sample

80 g of the dried, powdered plant material (ZSG root, stem, leaf; HLS; BLJ) were accurately weighed and extracted with

https://doi.org/10.25135/rnp.2607.3975
Rec. Nat. Prod. 2027, 21(2):e26073975

800 mL of distilled water (1:10, w/v) by heat refluxing for 1.5 hours. The extraction was repeated three times. After each extraction, the mixture was filtered through Whatman No. 1 filter paper (GE Healthcare, Chicago, IL, USA). The three filtrates were combined and concentrated under reduced pressure using a rotary evaporator (Büchi R-300, Flawil, Switzerland) at 60°C until a viscous syrup was obtained. The concentrated extract was then lyophilized (freeze-dried) for 48 hours to obtain a dry powder. The dried extract was re-dissolved in distilled water to a final concentration of 1 g crude drug equivalent per mL (1 g/mL) and stored at −20°C for subsequent administration.

2.2.1.2 Animal Experiment

After the experimental rats were adaptively fed for 7 days, the 36 rats were randomly divided into six groups (n = 6 per group): a control group (healthy group), ZSG root extract group, ZSG stem extract group, ZSG leaf extract group, HLS extract group, and BLJ extract group. According to the established ammonia-induced acute pharyngitis model protocol described in *Pharmacological Methods of Traditional Chinese Medicine* (Wei et al., 2022) an acute pharyngitis rat model was established. Except for the control group, the acute pharyngitis model was induced by spraying the 15% ammonia water 2 times a day (once in the morning and once in the afternoon), 3 puffs each time, for 4 consecutive days. At the same time, the control group received an equal volume of 0.9% sterile saline sprayed under the same conditions. During the experiment, the degree of yellowing hair, severity of hair loss, diet, body weight fluctuation, and whether death occurred in each group of rats were recorded, and the general status of each group of rats after modeling was carefully observed and recorded. From day 5 onwards, the respective herbal extracts (4.32 g/kg body weight) or an equal volume of saline were administered intragastrically once daily for 7 consecutive days (Wei et al., 2022). On the final day of administration, rats were fasted for 12 hours (with free access to water) to minimize dietary interference with serum metabolomics. Subsequently, the rats were deeply anesthetized by inhalation of diethyl ether in a sealed induction chamber. Anesthesia depth was confirmed by the loss of the pedal withdrawal reflex. The abdominal cavity was opened via a midline incision, and blood (approximately 5–6 mL per rat) was drawn from the abdominal aorta using a 10 mL syringe fitted with a 21-gauge needle. The blood was transferred to sterile centrifuge tubes without anticoagulant. The pharyngeal mucosal tissues were then carefully excised using the cricothyroid notch as an anatomical landmark, rinsed with ice-cold saline, snap-frozen in liquid nitrogen, and stored at −80°C for subsequent analyses. Finally, the rats were euthanized by exsanguination under deep anesthesia, followed by cervical dislocation to ensure death.

2.2.2 Sampling

Serum Preparation: Blood samples were allowed to clot at room temperature (25°C) for 30 minutes, then centrifuged at 3,000 rpm (approximately 1,500 × g) for 10 minutes at 4°C. The supernatant (serum) was carefully transferred into sterile 1.5 mL microcentrifuge tubes, divided into aliquots (200 µL each), and immediately stored at −80°C until LC-MS analysis.

Fecal Sample Collection: Fresh fecal pellets were collected directly from the rectum of each rat using sterile forceps, placed into sterile 2.0 mL microcentrifuge tubes, snap-frozen in liquid nitrogen within 5 minutes of collection, and stored at −80°C for subsequent DNA extraction and 16S rRNA sequencing.

For LC-MS analysis, frozen serum samples were thawed on ice. An aliquot of 100 µL of each serum sample was precisely transferred to a 1.5 mL centrifuge tube. Then, 400 µL of ice-cold extraction solution (methanol:acetonitrile = 1:1, v/v) containing four internal standards (including L-2-chlorophenylalanine at 0.02 mg/mL, camphor-10-sulfonic acid at 0.01 mg/mL, and two additional isotopically labeled internal standards) was added to each tube. The mixture was vortexed for 30 seconds using a digital vortex mixer at 2,500 rpm and subjected to low-temperature ultrasonic extraction for 30 minutes (5°C, 40 kHz). Subsequently, the sample was placed at −20°C for 30 minutes to precipitate proteins and centrifuged for 15 minutes (13,000g, 4°C). The supernatant was transferred and dried under nitrogen gas. Then, 100 µL of reconstitution solution (acetonitrile:water = 1:1, v/v) was added to reconstitute the residue. The solution was vortexed for 30 seconds and underwent low-temperature ultrasonic extraction for 5 minutes (5°C, 40 kHz). After centrifugation at 13,000 × g for 10 minutes at 4°C, the final supernatant was transferred to autosampler vials with 250 µL glass inserts for LC-MS analysis. A pooled quality control (QC) sample was prepared by mixing 20 µL of the supernatant from each individual sample and processed identically to the test samples.

2.2.3 LC-MS Detection

The LC-MS analysis was performed on a Thermo Scientific™ UHPLC-Q Exactive™ system, which combines ultrahigh performance liquid chromatography with a Q Exactive hybrid quadrupole-Orbitrap mass spectrometer. Chromatographic separation was achieved using an ACQUITY UPLC BEH C18 column (100 mm × 2.1 mm, 1.7 µM; Waters, Milford, USA) maintained at 40°C. The mobile phase consisted of (A) water with 0.1% formic acid and 2% acetonitrile, and (B) acetonitrile with 0.1% formic acid. The flow rate was 0.40 mL/min and the injection volume was 3 µL. The mass spectrometric data were collected using a Thermo UHPLC-Q Exactive HF-X. Mass spectrometric detection was carried out using electrospray ionization (ESI) in both positive and negative ion modes. Key MS parameters were set as follows: scan range, 70–1050 m/z; sheath gas flow, 50 arb; auxiliary gas flow, 13 arb; heater temperature, 450°C; capillary temperature, 320°C; spray voltage, +3500 V (positive) and −3000 V (negative); S-Lens RF level, 40; normalized collision energy, 20–40–60 eV (stepped); resolution, 70,000 for full MS and 17,500 for MS^2. Data acquisition was performed with the Data Dependent Acquisition (DDA) mode. Since absolute quantification was not performed, the relative contents (expressed

as peak areas) of the identified secondary metabolites from the plant sources are presented in Supplementary Table S1, while those detected in the collected animal samples are presented in Supplementary Table S2.

2.2.4 Quality Control

To ensure analytical stability and reproducibility, QC samples were injected every 5–10 analytical samples throughout the entire run. The QC samples were used to monitor instrument performance, retention time shifts, and signal intensity variations. Peaks with a coefficient of variation (RSD) of the integrated peak areas greater than 30% in QC samples were excluded from further analysis. As shown in Supplementary Table S1, the RSDs for the majority of the detected metabolites were below 30%, confirming the reliability and reproducibility of the analytical method. Since absolute quantification was not performed, the relative content of each identified metabolite is expressed as its normalized peak area, which allowed for semi-quantitative comparison across different sample groups (see Supplementary Tables S1 and S2). Blank samples (extraction solution without serum) were also analyzed to identify and exclude potential background contaminants.

2.2.5 Screening of Active Ingredients

The components detected in rat serum after oral administration of ZSG/HLS/BLJ were considered as the potential absorbed bioactive constituents and were used for subsequent network pharmacology analysis. The SMILES number of each blood component was copied into the Swiss ADME platform (www.swissadme.ch) for screening. Key pharmacokinetic indicators were evaluated, including gastrointestinal absorption (GI absorption), which was required to be "high". A component was considered an active ingredient only if at least two indicators returned a "yes" result.

2.2.6 Targets prediction of herbs' components

The SMILES numbers of the drug components identified in Section 2.2 were entered into the Swiss Target Prediction database (www.swisstargetprediction.ch). Upon entry, the molecular structures of the components were displayed on the right side of the interface. After selecting the relevant species, the prediction was initiated. The results were exported to Excel, and targets with a Probability ≥0.1 were selected. Relevant information including target names, common names, and Uniprot IDs was extracted. Disease-related targets were obtained by searching the GeneCards database (www.genecards.org) and the OMIM database (www.omim.org) using the keyword "Pharyngitis". The resulting targets constituted the pharyngitis-related target dataset. The Venny online tool (https://bioinfogp.cnb.csic.es/tools/venny/) was used to identify the intersection between the targets of the active components from ZSG and HLS and the pharyngitis-related targets. The overlapping targets obtained from this analysis represent the potential targets through which ZSG and HLS exert anti-pharyngitis effects.

2.2.7 Construction of Protein-Protein Interaction (PPI) Networks

The protein-protein interaction (PPI) network was constructed using the STRING database (cn.string-db.org). The "multiple proteins" mode was selected, with the protein species set to "*Homo sapiens*". Potential therapeutic targets for pharyngitis were input, and a confidence score threshold of 0.900 was applied to generate the PPI map. The resulting data were exported in TSV format and imported into Cytoscape software for visual analysis and generation of a PPI network topology graph. Additionally, a drug-component-target gene network diagram was constructed to visualize the interactions.

2.2.8 Enrichment Analysis of GO and KEGG Pathways

The intersecting genes among ZSG, HLS and BLJ were imported into the DAVID database (https://davidbioinformatics.nih.gov/). After selecting "OFFICIAL_GENE_SYMBOL" and restricting the species to *Homo sapiens*, GO and KEGG functional enrichment analyses were performed with appropriate parameter settings. The GO analysis encompassed biological process (BP), cellular component (CC), and molecular function (MF). The enrichment results were then imported into the Bioinformatics Platform (https://www.bioinformatics.com.cn/) to generate bubble charts for visualization.

2.2.9 Metscape Database Enrichment

The intersecting genes were imported into the Metascape database (https://metascape.org/gp/index.html#/main/step1) for enrichment analysis.

2.2.10 Molecular Docking

Genes were selected for molecular docking based on their involvement in relevant pathways. Protein receptor structures were downloaded in PDB format from the RCSB PDB database (https://www.rcsb.org/), the corresponding PDB IDs were summarized in Table 1**,** and the 3D structures of small-molecule ligands were obtained in SDF format from PubChem (https://pubchem.ncbi.nlm.nih.gov/). The SDF files were then converted to PDB format using Open Babel. The prepared protein structures were imported into AutoDock Tools 1.5.7, where water molecules were added and hydrogen atoms were removed before saving the processed files. For the small molecules, hydrogen atoms were added and the structures were energy-minimized and saved for docking. In the initial screening stage, a blind docking approach was performed using a larger grid box to identify potential binding pockets across the entire protein surface (Supplementary of blind docking). Subsequently, to improve the accuracy of the binding modes and binding energies, the active binding sites were identified using the deep learning-based tool DeepSite. This tool predicts druggable pockets and provides specific coordinates for the binding center. Except MPO, the active binding sites of the proteins were defined by grid boxes centered at specific X, Y, and Z coordinates (Hu et al., 2027): TNF (−39.85, −72.23, 60.22), CASP1 (13.64, 1.80,

https://doi.org/10.25135/rnp.2607.3975
Rec. Nat. Prod. 2027, 21(2):e26073975

Table 1. PDB IDs of all target proteins

Protein	PDB ID	Resolution	Organism(s)
CASP1	8WRA	1.45 Å	*Homo sapiens*
JAK3	3LXK	2.00 Å	*Homo sapiens*
MPO	8CVQ	1.65 Å	*Homo sapiens*
PIK3CA	7R9V	2.69 Å	*Homo sapiens*
SRC	8BQ3	2.66 Å	*Homo sapiens*, synthetic construct
TNF	4E4S	1.95 Å	*Ochotona princeps*
XIAP	4KMP	1.95 Å	*Homo sapiens*
EP300	7SMD	2.15 Å	*Homo sapiens*
IL6	7PHS	2.77 Å	*Homo sapiens*
JAK2	7F7W	1.83 Å	*Homo sapiens*
STAT3	6NJS	2.70 Å	*Homo sapiens*

19.19), JAK3 (−1.12, 15.81, 4.11), PIK3CA (−1.79, −7.88, 13.43), SRC (11.36, 12.92, −12.72), XIAP (14.65, 0.0, 0.61), EP300 (10.35, 11.17, 12.77), IL6 (9.47, −32.18, 38.88), JAK2 (2.60, −12.22, 18.43), STAT3 (0.93, 26.96, 25.86) with dimensions of 60 × 60 × 60 Å, encompassing the entire active pocket. A binding energy of < −5 kcal/mol was considered indicative of good receptor-ligand affinity (Weigang et al., 2025). Selected docking poses were subjected to visualization and analysis using PyMOL 2.5 software.

2.2.11 Intestinal Flora Analysis

After the experiment, feces of rats in each group were collected in a sterile bench and stored in a −80°C refrigerator. 0.5 g of fecal samples were taken for detection of intestinal microorganisms by 16SrDNA high-throughput sequencing technology. Total microbial genomic DNA was extracted from 42 samples using the FastPure Stool DNA Isolation Kit (MJYH, shanghai, China) according to manufacturer's instructions. The quality and concentration of DNA were determined by 1.0% agarose gel electrophoresis and a NanoDrop® ND-2000 spectrophotometer (Thermo Scientific Inc., USA) and kept at −80°C prior to further use. The hypervariable region V3-V4 of the bacterial 16S rRNA gene were amplified with primer pairs 338F (5′-ACTCCTACGGGAGGCAGCAG-3′) and 806R (5′-GGACTACHVGGGTWTCTAAT-3′) by an T100 Thermal Cycler (BIO-RAD, USA). And the specific operations were completed by Shanghai Majorbio Biotechnology Co., Ltd. For the obtained raw data, sequence splicing, data optimization and ASV denoising were carried out to obtain effective data. Sequences were classified according to 97% similarity to generate operational taxonomic units (OTUs). All data analyses were performed on the Majorbio Cloud Platform (https://cloud.majorbio.com) as follows: Alpha diversity indices such as Chao 1 and Shannon index were calculated using mothur software (http://www.mothur.org/wiki/Calculators), and Kruskal-Wallis rank sum test was used for intergroup difference analysis of Alpha diversity; PCoA analysis based on bray-curtis distance algorithm was used to test the similarity of microbial community structure among samples; LEfSe analysis (http://huttenhower.sph.harvard.edu/LEfSe) (LDA > 2, P < 0.05) was used to determine the bacterial groups with significantly different abundances from phylum to genus levels between different groups; and community composition analysis based on Python was used to obtain the microbial composition from phylum to genus levels.

3 Results and Analysis

3.1 Drug Active Ingredients

The actives of the root, stem, leaf of ZSG, HLS *and* BLJ were summarized in Table 2–6, respectively. 8 active substances were obtained by screening the blood components of ZSG roots through Swiss ADME; 11 active substances were obtained by screening the blood components of ZSG stems through Swiss ADME; 8 active substances were obtained by screening the blood components of ZSG leaves through Swiss ADME; 4 active substances were obtained by screening the blood components of HLS through Swiss ADME; 6 active substances were obtained by screening the blood components of BLJ through Swiss ADME. Some minor components detected in the serum such as acetophenone, p-tolualdehyde may originate from environmental, microbial, or dietary sources rather than directly from the herbal extracts, and are therefore not listed in the table. Figure 1 was the positive and negative ion flow diagram of the drug.

3.2 Potential Anti-Pharyngitis Targets of the Drug

Through the SwissTarget Prediction database, the total number of predicted targets for active components in the roots of ZSG was 267; the total number of targets for active components in the stems of ZSG was 394; the total number of targets for active components in the leaves of ZSG was 375; the total number of predicted targets for active components in HLS was 198; and the total number of predicted targets for active components in BLJ was 261. Relevant targets for pharyngitis were obtained from the Gene Cards and OMIM databases. The median of the source values was calculated using the MEDIAN formula as 1.605020404, and genes greater than or equal to this median were retained, ultimately yielding 746 disease-related genes. Subsequently, the Venny software was

Table 2. Active components at the root of ZSG

Metabolite	m/z	Adducts	Formula
16-Hydroxyhexadecanoic acid	290.2685	M^+NH_4	$C_{16}H_{32}O_3$
7-methoxycoumarin	177.0545	M^+H	$C_{10}H_8O_3$
Alantolactone	233.1534	M^+H	$C_{15}H_{20}O_2$
Embelin	293.1756	M^-H	$C_{17}H_{26}O_4$
MG(a-15:0/0:0/0:0)[rac]	334.2947	M^+NH_4	$C_{18}H_{36}O_4$
Myristoleic acid	191.1792	$M^+H^-{}_2H_2O$	$C_{14}H_{26}O_2$
Quercetin	301.0354	—	$C_{15}H_{10}O_7$
Rapanone	—	—	—

Note: The "—" indicates that no data is available for the corresponding items.

Table 3. Active components at the stem of ZSG

Metabolite	m/z	Adducts	Formula
7-methoxycoumarin	177.0545	M^+H	$C_{10}H_8O_3$
9,10,13-TriHOME	329.2332	M^-H	$C_{18}H_{34}O_5$
Alantolactone	233.1534	M^+H	$C_{15}H_{20}O_2$
Artemisinin	265.1432	$M^+H^-H_2O$	$C_{15}H_{22}O_5$
Embelin	293.1756	M^-H	$C_{17}H_{26}O_4$
Fisetin	287.0546	M^+H	$C_{15}H_{10}O_6$
Gamma-cehc	263.1287	M^-H	$C_{15}H_{20}O_4$
Orcinol	125.0599	M^+H	$C_7H_8O_2$
Salvigenin	361.1276	$M^+CH_3OH^+H$	$C_{18}H_{16}O_6$
Sparanone A	223.0607	M^-H	$C_{11}H_{12}O_5$
Tianshic acid	329.2332	M^-H	$C_{18}H_{34}O_5$

Table 4. Active components at the leaf of ZSG

Metabolite	m/z	Adducts	Formula
7-methoxycoumarin	177.0545	M^+H	$C_{10}H_8O_3$
9,10,13-TriHOME	329.2332	M^-H	$C_{18}H_{34}O_5$
Alantolactone	233.1534	M^+H	$C_{15}H_{20}O_2$
Artemisinin	265.1432	$M^+H^-H_2O$	$C_{15}H_{22}O_5$
Embelin	293.1756	M^-H	$C_{17}H_{26}O_4$
Fisetin	287.0546	M^+H	$C_{15}H_{10}O_6$
Kaempferol	287.0545	M^+H	$C_{15}H_{10}O_6$
Orcinol	125.0599	M^+H	$C_7H_8O_2$

Table 5. Active components of HLS

Metabolite	m/z	Adducts	Formula
7-methoxycoumarin	177.0545	M^+H	$C_{10}H_8O_3$
9,10,13-TriHOME	329.2332	M^-H	$C_{18}H_{34}O_5$
Embelin	293.1756	M^-H	$C_{17}H_{26}O_4$
Orcinol	125.0599	M^+H	$C_7H_8O_2$

used to intersect the targets of active components from ZSG, HLS, and pharyngitis-related targets. As shown in Figure 2, the potential targets for anti-pharyngitis activity were determined as follows, 22 in the roots of ZSG, 28 in the stems of ZSG, 24 in the leaves of ZSG, 21 in HLS, and 29 in BLJ.

Table 6. Active components of BLJ

Metabolite	m/z	Adducts	Formula
(+)-Syringaresinol	419.1694	M^+H	$C_{22}H_{26}O_8$
7-methoxycoumarin	177.0545	M^+H	$C_{10}H_8O_3$
Bellidifolin	319.0458	M^+FA^-H	$C_{14}H_{10}O_6$
Embelin	293.1756	M^-H	$C_{17}H_{26}O_4$
Fisetin	287.0545	M^+H	$C_{15}H_{10}O_6$
Orcinol	125.0599	M^+H	$C_7H_8O_2$

3.3 PPI Network Map and Drug-Component-Target Gene Map

As shown in Figure 3, the drug-component-target gene maps and PPI maps of ZSG, HLS, and BLJ were presented. Using Cytoscape, drug-component-target gene maps were drawn based on drugs, active components, and intersecting genes. Specifically, ZSG had 54 nodes and 83 edges; HLS had 28 nodes and 29 edges; and BLJ had 38 nodes and 44 edges. Furthermore, STRING results were imported into Cytoscape to construct PPI networks. ZSG had 27 nodes and 48 edges; HLS had 17 nodes and 35 edges; and BLJ had 24 nodes and 61 edges. In the networks, larger nodes with colors ranging from yellow to green indicate higher degree values of targets. Notably, targets such as SRC, TNF, PIK3CA, STAT3, AKT1, EGFR, PTPN11, PIK3CD, and JAK2 are located at the

https://doi.org/10.25135/rnp.2607.3975
Rec. Nat. Prod. 2027, 21(2):e26073975

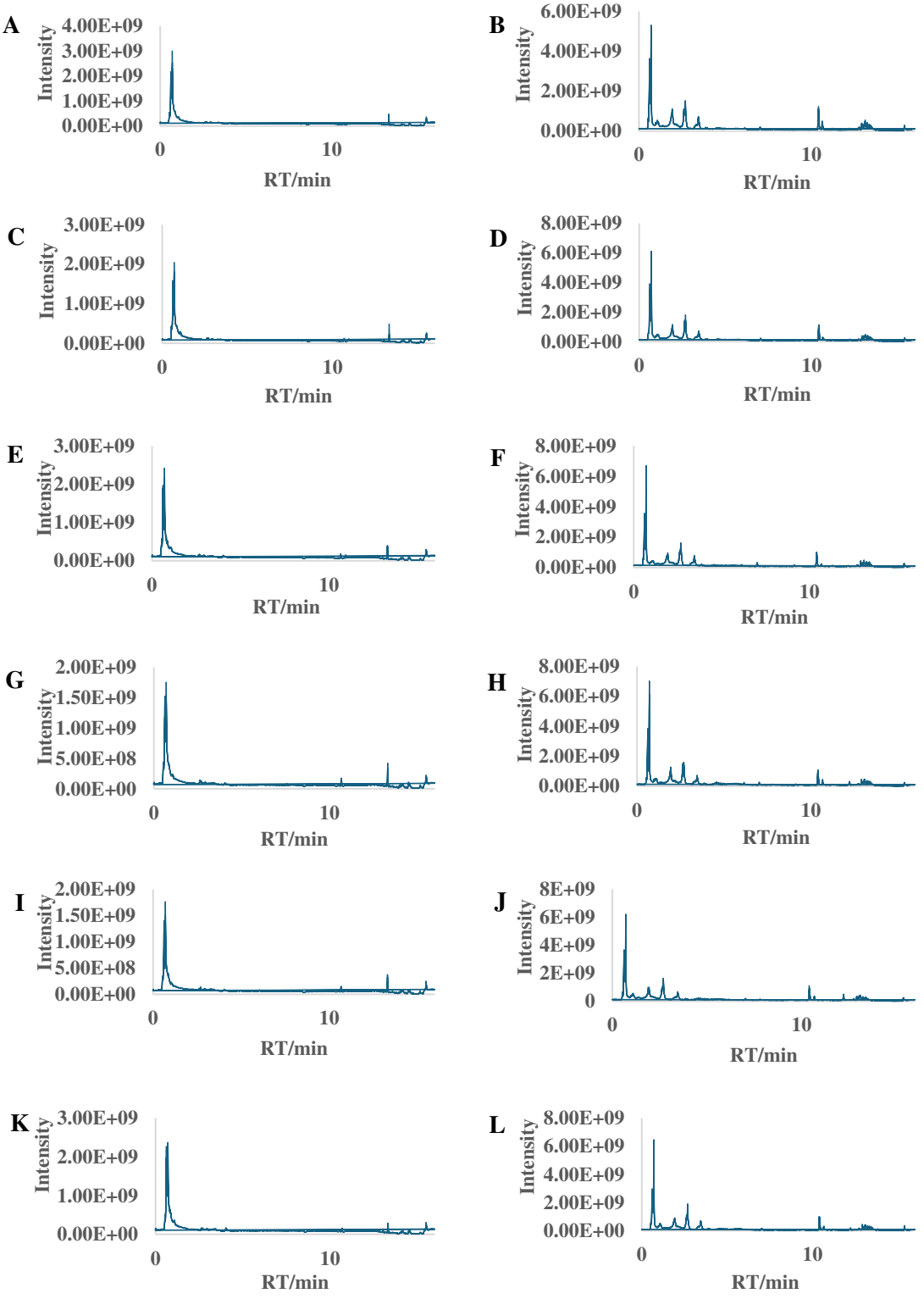


Figure 1. Positive and negative ion current diagrams. Negative ion flow diagram of root (A), stem (C), and leaves (E) of ZSG, HLS (G), and BLJ (I); Positive ion flow diagram of root (B), stem (D), and leaves (F) of ZSG, HLS (H), and BLJ (J). MC negative ion flow diagram (K); MC positive ion flow diagram (L)

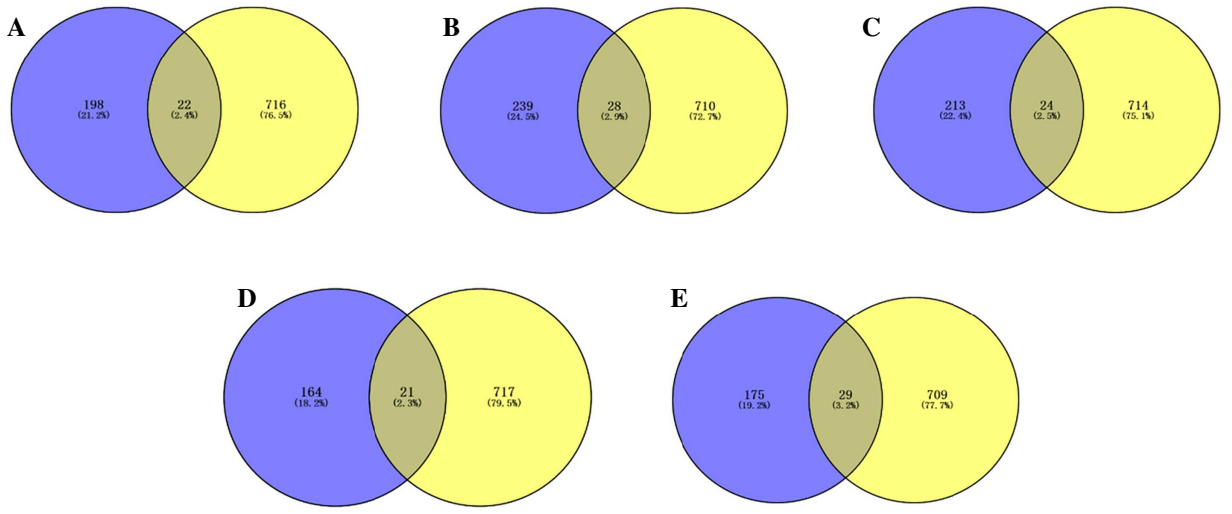


Figure 2. Venny diagram of drugs and diseases. Venny diagram of the root (A), stem (B), and leaf (C) of ZSG, HLS (D), and BLJ (E) and pharyngitis

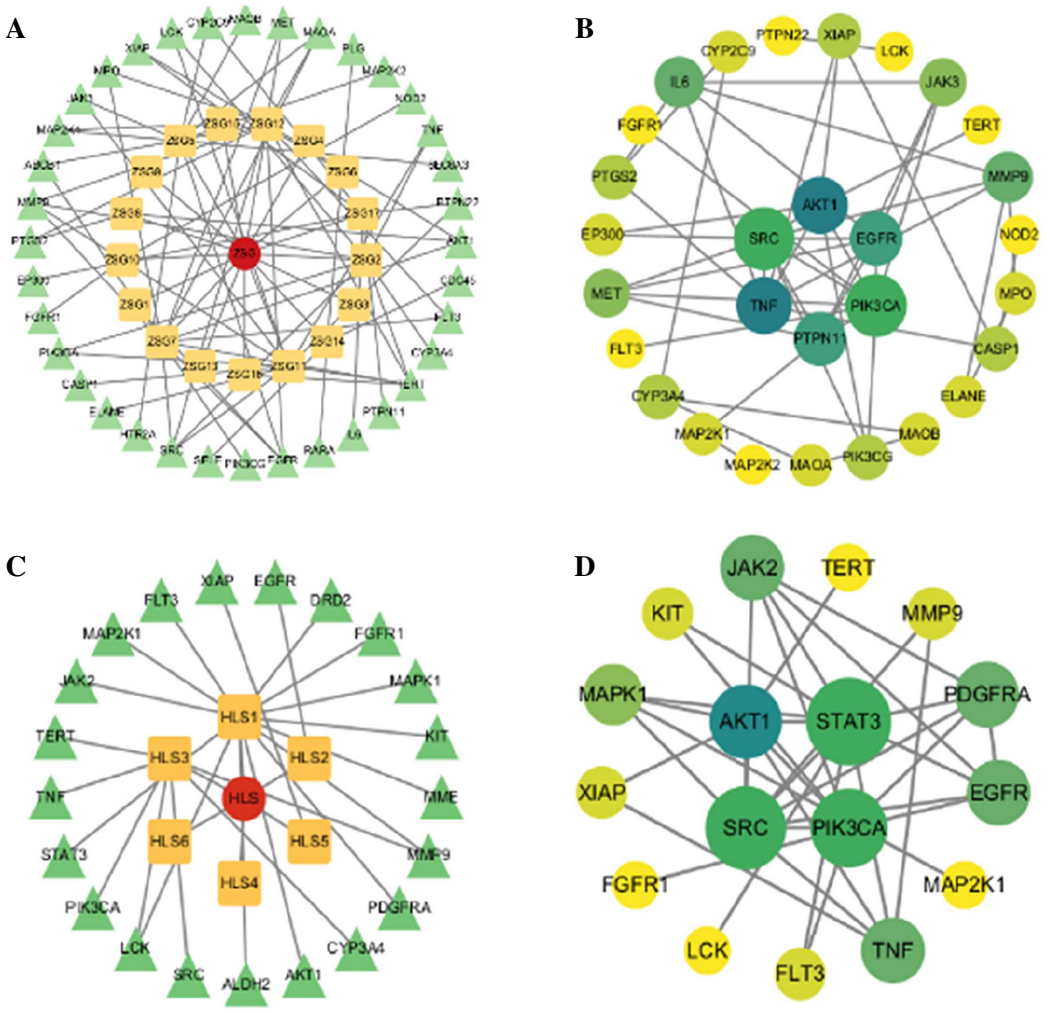


Figure 3. (Continued)

https://doi.org/10.25135/rnp.2607.3975
Rec. Nat. Prod. 2027, 21(2):e26073975

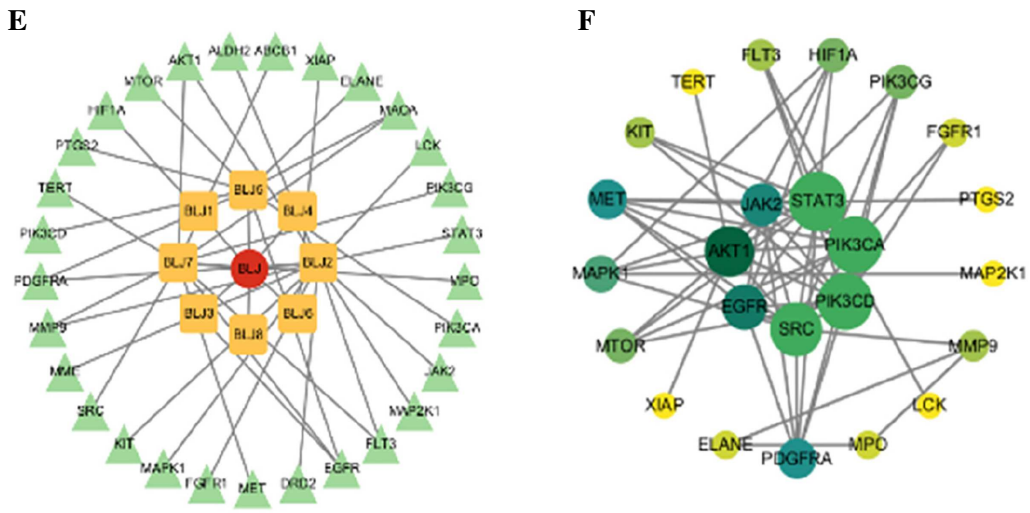


Figure 3. PPI network diagram and drug component target gene diagram. Drug component-Target gene map of ZSG (A), HLS (C), and BLJ (E); PPI network diagrams of ZSG (B), HLS (D), and BLJ (F)

core of the networks, playing crucial regulatory roles in the PPI networks.

3.4 GO and KEGG

After screening, the roots of ZSG yielded 133 biological process (BP) entries, 50 molecular function (MF) entries, 18 cellular component (CC) entries, and 81 KEGG pathways. The stems of ZSG had 190 BP entries, 87 MF entries, 27 CC entries, and 116 KEGG pathways. The leaves of ZSG contained 163 BP entries, 82 MF entries, 22 CC entries, and 122 KEGG pathways. HLS had 186 BP entries, 47 MF entries, 24 CC entries, and 119 KEGG pathways. BLJ yielded 225 BP entries, 78 MF entries, 31 CC entries, and 132 KEGG pathways. The top 10 entries of BP, CC, MF, and KEGG were selected based on the abundance value, and the results were imported into Bioinformatics Platform to generate a scatter plot as shown in Figure 4. The size of the points indicates the count value, and the color indicates the *p*-value.

3.5 Molecular Docking

Molecular docking of the drug's active components with targets yielded docking energies, the active binding sites of the proteins were defined by grid boxes centered at specific X, Y, and Z coordinates (seen in Table 7–10). Then, the docking results with stronger binding ability were selected for visualization analysis (see Figure 5). Generally, a binding energy < −5 kcal/mol indicates good affinity between the receptor and ligand. The results show that there is a stable binding ability between the drug's active components and targets. As shown in Figure 5, the active small molecules of drugs like ZSG are connected to the target proteins via hydrogen bonds, which improves the binding stability between the ligand and the receptor. The results of the global blind docking are shown in Supplementary blind docking.

3.6 Intestinal Flora Analysis

3.6.1 α and β diversity analysis

According to the sparsity curve (Figure 6C), the sequencing depth is sufficient and the richness is similar, indicating a high detection rate of microorganisms in the samples, which meets the standards for sequencing and database analysis. To evaluate the overall gut microbiota health and dysbiosis status, the GMHI index and microbiota dysbiosis index were calculated. As shown in Figure 6A, B, the model group exhibited a significant shift in these indices compared to the control group. As shown in Figure 6E–I, compared with the control group, the Sobs, Chao, Ace, and Shannon indices in the model group were significantly increased, while the Simpson index was significantly decreased. Compared with the model group, Root, Stem, HLS, and BLJ significantly down-regulated the Sobs, Chao, Ace, and Shannon indices and up-regulated the Simpson index, indicating that Root, Stem, HLS, and BLJ have certain effects on the richness, evenness, and diversity of intestinal flora species in rats. PCoA and NMDS analyses were used to evaluate the differences between microbial communities in each group. The *β*-diversity results are shown in Figure 7A, B. The differential flora between the control group and the model group showed separation, indicating obvious differences in the flora structure between the two groups. At the same time, Root, Stem, etc., were significantly distinguished from the model group samples and tended to the control group, indicating that the intestinal flora structure of rats in the Root, Stem, etc., groups was redirected to the control group.

3.6.2 Analysis of Species Composition at Different Taxonomic Levels

The phylum-level difference analysis is shown in Figure 7E. Compared with the control group, the relative abundance of Firmicutes in the model group increased, while the relative abundances of Bacteroidetes, Proteobacteria,

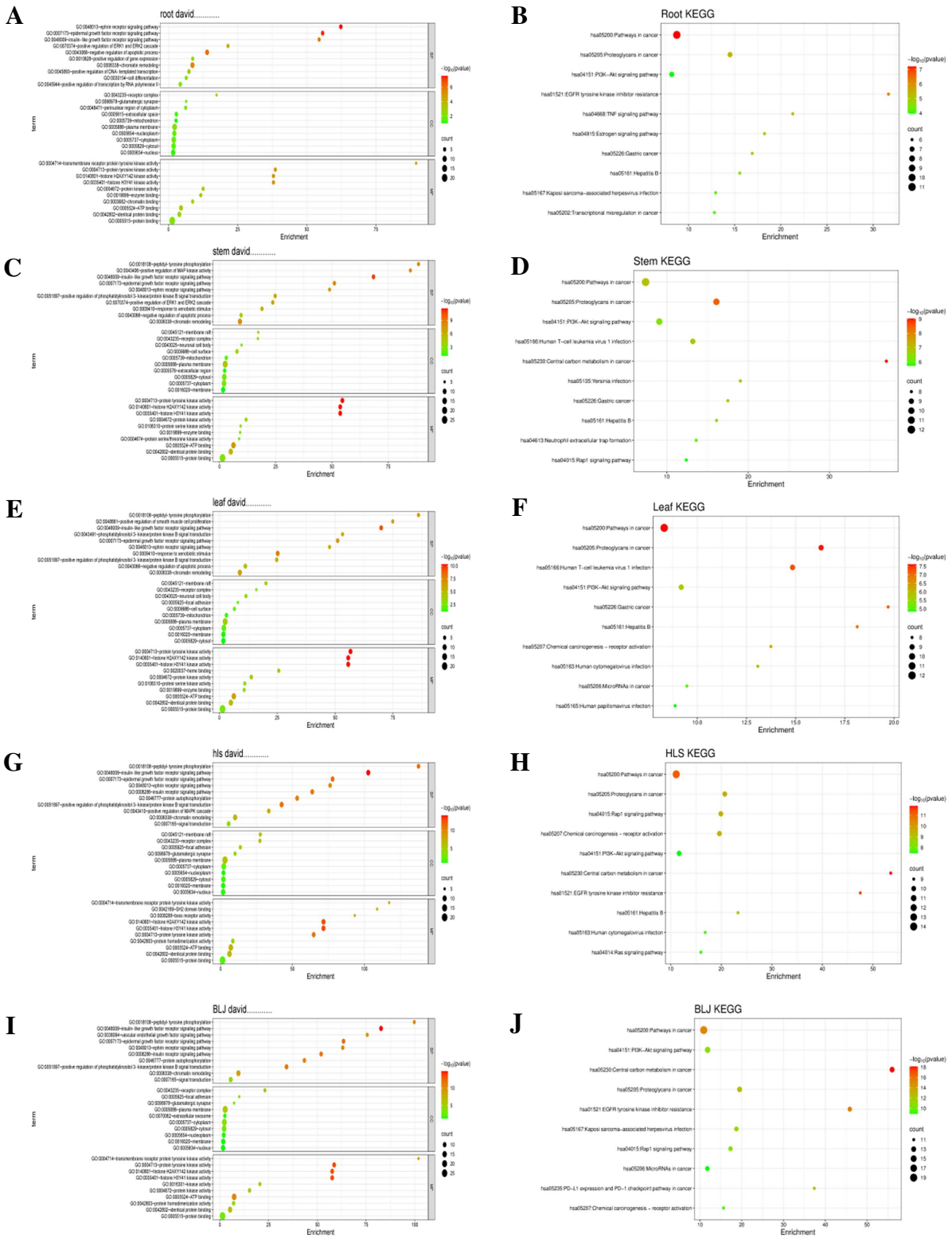


Figure 4. Scatter plot of drug bubbles. GO enrichment analysis of the anti-pharyngitis ability of root (A), stem (B), and leaves (C) of ZSG, HLS (D), and BLJ (E); KEGG enrichment analysis of the anti-pharyngitis ability of root (F), stem (G), and leaves (H) of ZSG, HLS (I), and BLJ (J)

https://doi.org/10.25135/rnp.2607.3975
Rec. Nat. Prod. 2027, 21(2):e26073975

Table 7. Docking and binding energy of ZSG

Active components	Binding energy/(kcal/mol)					
	CASP1	JAK3	MPO	PIK3CA	SRC	TNF
Alantolactone	−6.56	−5.84	−6.20	−6.24	−5.95	−6.32
Artemisinin	−8.23	−6.80	−6.54	−7.45	−6.77	−7.83
Embelin	−5.43	−4.99	−2.89	−5.77	−4.78	−4.86
Fisetin	−6.31	−6.77	−4.73	−7.58	−6.09	−6.17
Orcinol	−5.42	−5.20	−4.88	−4.15	−4.01	−4.78
Salvigenin	−6.23	−6.40	−2.14	−6.35	−6.40	−6.67
Tianshicacid	−3.62	−4.57	−4.21	−4.48	−3.90	−4.58
Kaempferol	−6.01	−6.56	−5.02	−6.17	−5.67	−6.16
Myristoleic acid	—	—	−4.00	—	—	—
Quercetin	—	—	−4.04	—	—	—
Rapanone	—	—	−2.99	—	—	—

Note: The "—" indicates that no data is available for the corresponding items.

Table 8. Docking and binding energy of ZSG (continued)

Active components	Binding energy/(kcal/mol)		
	XIAP	EP300	IL6
Alantolactone	−6.28	−6.01	−6.46
Artemisinin	−6.93	—	—
Embelin	−5.0	−3.96	−4.75
Fisetin	−6.56	—	—
Orcinol	−3.91	—	—
Salvigenin	−6.80	—	—
Tianshicacid	−4.76	—	—
Kaempferol	−7.44	—	—
Myristoleic acid	−4.79	−4.03	−5.17
Quercetin	−7.31	−6.08	−6.60
Rapanone	−4.63	−4.02	−4.83

Note: The "—" indicates that no data is available for the corresponding items.

Table 9. Docking and binding energy of HLS

Active components	Binding energy/(kcal/mol)			
	PIK3CA	SRC	TNF	XIAP
Embelin	−5.77	−4.78	−4.86	−5.0
Orcinol	−4.15	−4.01	−4.78	−3.91

and Actinobacteria decreased. After drug intervention, Bacteroidetes was significantly redirected, and except for HLS, other drugs significantly redirected Firmicutes. The family-level difference analysis is shown in Figure 7F. Compared with the control group, the relative abundances of Lachnospiraceae and Lactobacillaceae in the model group increased, but the Muribaculaceae decreased. After BLJ, HLS, and Root intervention, Lachnospiraceae was significantly redirected, and after BLJ, HLS, Stem,

Table 10. Docking and binding energy of BLJ

Active components	Binding energy/(kcal/mol)					
	JAK2	MPO	XIAP	PIK3CA	SRC	STAT3
Embelin	−4.86	−2.89	−5.0	−5.77	−4.78	−5.58
Fisetin	−6.68	−4.73	−6.56	−7.58	−6.09	−6.73
Orcinol	−3.9	−4.88	−3.91	−4.15	−4.01	−4.41

and Root intervention, Muribaculaceae was significantly redirected. After Leaf intervention Lactobacillaceae was significantly redirected. The genus-level results are shown in Figure 7G. Compared with the control group, the relative abundance of *norank_f__Muribaculaceae* in the model group decreased, while the relative abundances of *Lactobacillus* and *unclassified_f__Lachnospiraceae* increased. Except for HLS, other drugs significantly redirected *norank_f__Muribaculaceae*; Leaf intervention significantly redirected *Lactobacillus*; and drug intervention significantly redirected *unclassified_f__Lachnospiraceae*. These results indicated that BLJ, HLS, Stem, Root, and Leaf can regulate intestinal flora disorders in rats to a certain extent, promoting them to return to a normal physiological state.

3.6.3 LEfSe Analysis

The LEfSe multi-level species hierarchy tree diagram further displays the differences of species at different taxonomic levels in the form of a phylogenetic tree diagram. The circles from the inside to the outside represent the taxonomic levels from phylum to genus, as shown in Figure 7C. As shown in Figure 7D, the characteristic flora of the control group, such as *Bifidobacterium*, *Verrucomicrobiota*, and *Peptostreptococcaceae*, etc., showed significant differences in abundance. The significantly different flora in the model group were *Erysipelotrichaceae*, *Turicibacter*, and *Erysipelotrichales*. Those in the Root group were *Alloprevotella*, *Burkholderiales* etc., those in the Stem group were

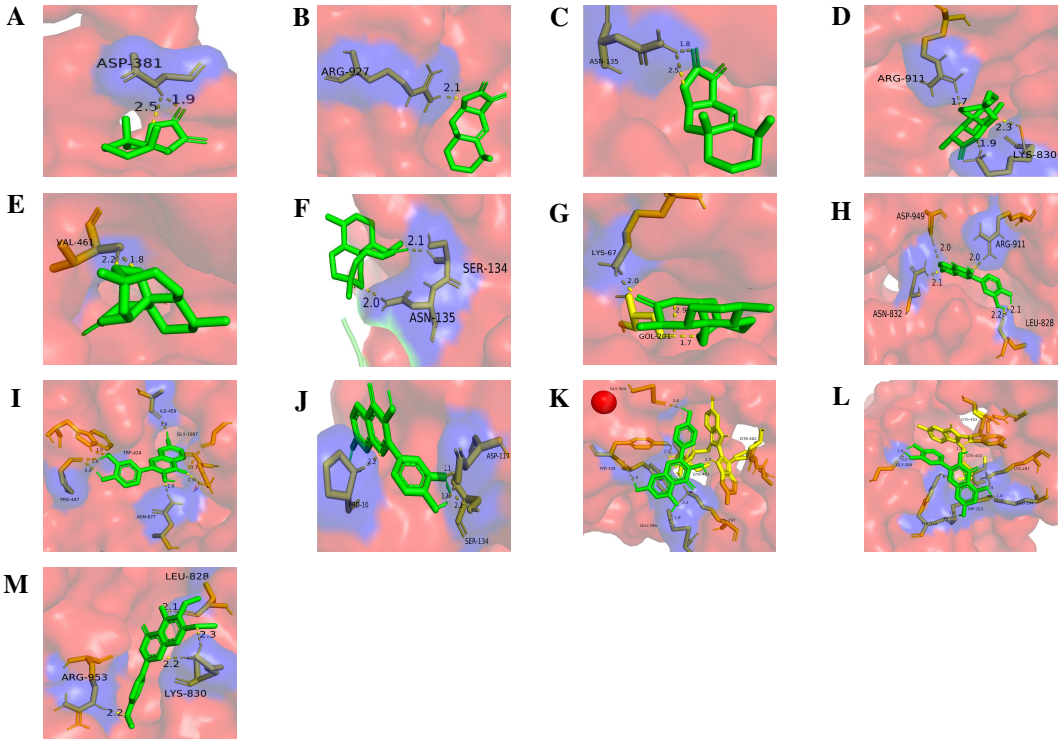


Figure 5. Molecular docking mode diagram. A. molecular docking mode diagram of AlantolactoneCASP1; B. molecular docking mode diagram of Alantolactone and EP300; C. molecular docking mode diagram of Alantolactone and SRC; D. molecular docking mode diagram of Artemisinin and JAK3; E. molecular docking mode diagram of Artemisinin and PIK3CA; F. molecular docking mode diagram of Artemisinin and SRC; G. molecular docking mode diagram of Artemisinin and TNF; H. molecular docking mode diagram of Fisetin and JAK3; I. molecular docking mode diagram of Fisetin and PIK3CA; J. molecular docking mode diagram of Fisetin and SRC; K. molecular docking mode diagram of Kaempfero and lXIAP; L. molecular docking mode diagram of Quercetin and XIAP; M. molecular docking mode diagram of Salvigenin and JAK3

Butyricicoccaceae, *Christensenellaceae* etc., and those in the Leaf group were Clostridia, etc. The significantly different flora in the HLS group was Firmicutes, those in the BLJ group were *Erysipelatoclostridium*, *Muribaculum*.

4 Discussion

This study uses network pharmacology and molecular docking techniques to explore the specific active components of ZSG, HLS, and BLJ, the targets of these active components, and the signaling pathways through which these medicinal materials exert their effects, providing certain reference value for subsequent studies on the mechanism of action of pharyngitis. In previous studies, the ZSG contains coumarins Chemical components such as Saponins, flavonoids, volatile oils, and phenols, quinones, cardiac glycosides, organic acids, tannins, amino acids, and sugars (Qing et al., 2022). The results of this study show that the active components of drugs such as ZSG in the treatment of pharyngitis are relatively complex, among which the more critical active components are Fisetin, Alantolactone, Kaempferol, Artemisinin, Embelin, and son on. Future studies using blank serum controls are needed to exclude potential contaminants. Fisetin has a variety of biological activities, including antioxidant, anti-inflammatory, anti-cancer, neuroprotective, and anti-aging effects (Shihao et al., 2024). In metabolic disorders, fisetin helps improve diabetic nephropathy and fatty liver degeneration caused by a high-fat diet. The anti-inflammatory and antioxidant effects of fisetin are expected to treat inflammatory diseases and reduce oxidative stress (Shihao et al., 2024). Multiple lines of evidence support that fisetin could suppress the PI3K/AKT pathway in different cells. Our conclusions are consistent with previous studies. We found that fisetin dosage-dependently blocked PI3K and AKT phosphorylation in ASMCs (Liu et al., 2024). Since it is well known that the PI3K/Akt signalling pathway is involved in the regulation of proinflammatory genes stimulating NF-κB activity (Cianciulli et al., 2016). Therefore, Fisetin has anti-inflammatory effects. Alantolactone exerts anti-inflammatory effects by preventing STAT1 phosphorylation in human immortalized epidermal cells (HaCaT cells), thereby interfering with the increase in RANTES and IL-8 induced by IFN-γ and tumor necrosis factor-α, and reducing the release of inflammatory factors. Studies have shown that dehydrocostus lactone inhibits LPS-induced inflammation by p38MAPK-dependent activation of hemoxygenase-1 in vitro and improves the survival rate of mice with sepsis induced by CLP (Yun, 2021). Studies have found that kaempferol can inhibit inflammatory responses by regulating the PI3K/AKT signaling pathway (Min et al., 2024), and

https://doi.org/10.25135/rnp.2607.3975
Rec. Nat. Prod. 2027, 21(2):e26073975

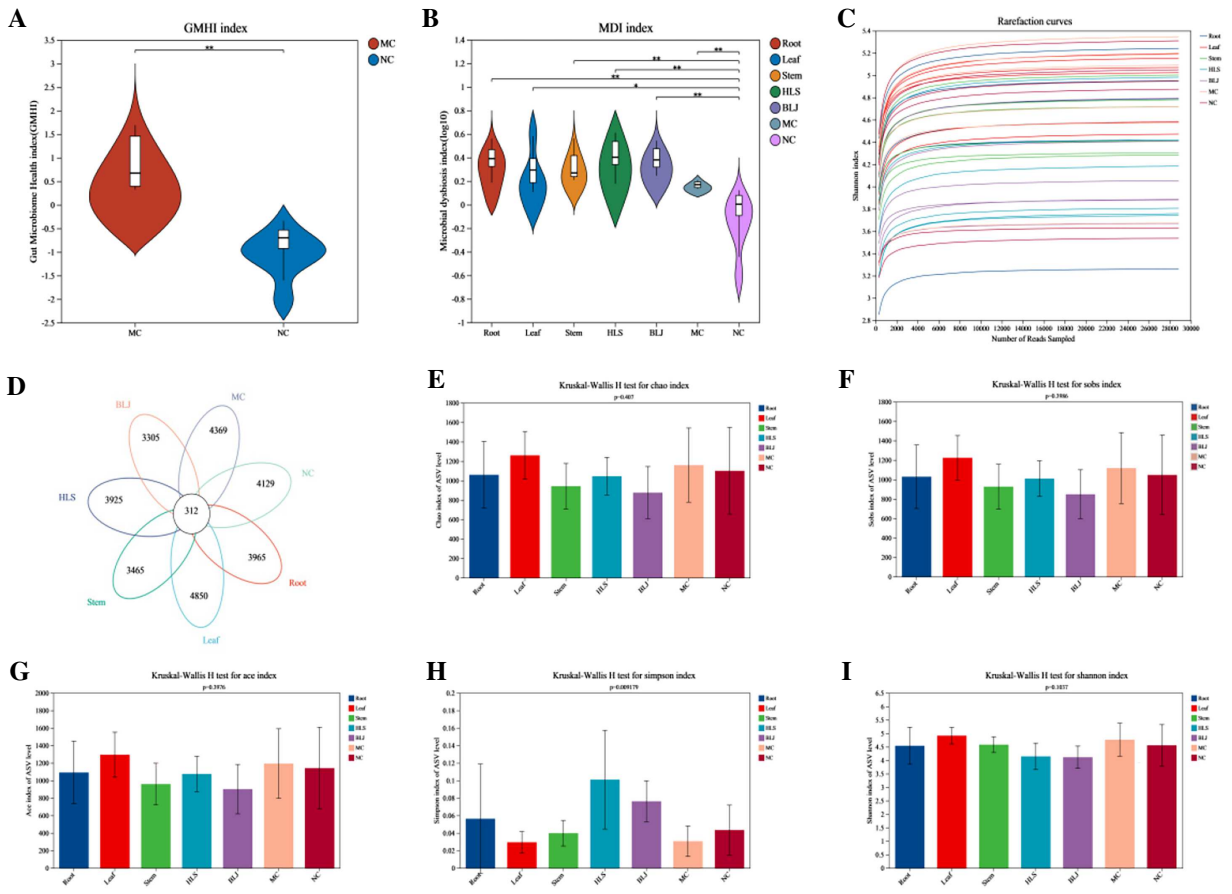


Figure 6. Gut microbiota analysis. A. Analysis chart of differences between GMHI index; B. Inter-group difference chart of microbiota dysbiosis index; C. Rarefaction attenuation curve; D. Venn chart; E–I. Test chart of differences between index groups

the results show that kaempferol can inhibit the activation of the PI3K/AKT signaling pathway. To further clarify the mechanism by which kaempferol regulates the PI3K/AKT signaling pathway to affect the progression of COPD, a study treated COPD model cells with the PI3K/AKT signaling pathway activator 740Y-P. The results showed that 740Y-P could reverse the effect of kaempferol on COPD model cells, reduce cell proliferation activity, promote cell apoptosis, and up-regulate the expression of inflammatory factors and ECM damage-related indicators, suggesting that kaempferol inhibits COPD inflammatory responses and ECM damage by suppressing the PI3K/AKT signaling pathway (Min et al., 2024). Artemisinin (ART) is an antimalarial drug isolated from *Artemisia annua* L. As a drug used in more than one million malarial patients, ART is demonstrated without noticeable side effects and adverse reaction (Yuan et al., 2019). Embelin demonstrates significant neuroprotective potential by inhibiting 5-LOX-mediated ferroptosis and oxidative stress, offering a promising therapeutic strategy for perinatal brain injury and related neurodevelopmental disorders (Zhang et al., 2025). The anti-inflammatory effects of artemisinin and analogs were attributed to the inhibition of TLRs and of key inflammatory signal transduction pathways that include NF-κB, syk tyrosine kinase, STAT1, -3, and -5, phosphoinoside 3-kinase (PI3K)/Akt, and mitogen-activated protein kinase (MAPK) (An et al., 2017). Through the Cytoscape protein-protein interaction network diagram, the core targets of drug treatment for pharyngitis were found to be SRC, TNF, PIK3CA, STAT3, JAK2, etc. TNF belongs to proinflammatory cytokines and mediates the TNF signaling pathway (Zaowei et al., 2025). The key target of the TNF signaling pathway is TNF-α, a critical inflammatory cytokine that can activate NF-κB to enter the nucleus and induce the expression of proinflammatory factors (TNF-α, IL-1, IL-6), chemokines (IL-8), and other genes to participate in immune and inflammatory responses. Multiple studies have shown that TNF-α expression is increased in the serum of patients or animals with chronic pharyngitis and decreases after treatment (Jin et al., 2025). Studies have shown that anti-inflammatory therapy is an effective strategy for treating pharyngitis and relieving throat itching and pain. The JAK2/STAT3 signaling pathway can regulate inflammatory cell differentiation, infiltration, and inflammatory factor expression. Inhibiting JAK2/STAT3 pathway activation can significantly reduce inflammatory responses (Yong et al., 2024). IL-6 is a multifunctional inflammatory cytokine and a key component of the inflammatory mediator network, playing an important role in inflammatory responses. It can play a cytoprotective and anti-inflammatory role in bacterial

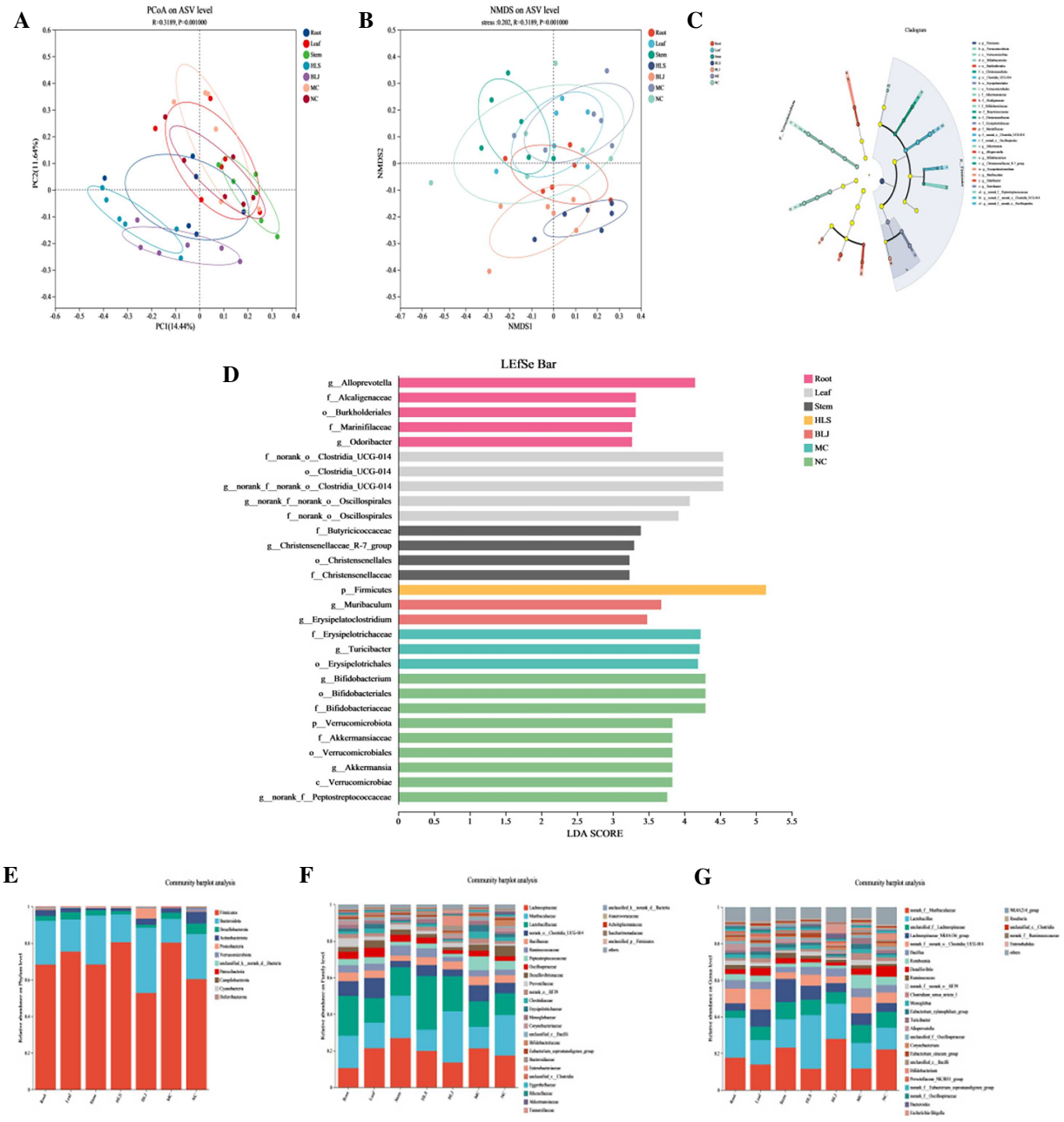


Figure 7. Gut microbiota structure analysis. A. PCoA Scatter plot analysis; B. NMDS scatter diagram; C. LEfSe multi-level species hierarchy tree diagram; D. LDA discrimination bar chart; E–G. Community bar chart

endotoxin-induced experimental lung injury by inhibiting macrophages from producing IL-1 and tumor necrosis factor (Heng et al., 2023). The results from KEGG and GO indicated that it mainly functions through the PI3K/AKT signaling pathway, Rap1 signaling pathway, Estrogen signaling pathway, and Ras signaling pathway etc. The data presented in this study reveal a new mechanism by which estrogens may influence the homeostasis of SC (Lustofin et al., 2025). The functions of Ras signaling pathway includes Implications for Wound Healing (Liu et al., 2022), Gout (Oh et al., 2021) and colorectal cancer (Sun et al., 2013) Molecular docking results show that active substances such as fisetin, costunolide, and kaempferol bind to core targets such as SRC, TNF, PIK3CA, STAT3, and JAK2 to treat pharyngitis.

Gut microbiota is the core commensal microorganism system of a human body, being considered as "the second genome" and the new "organ" (Yang et al., 2025). Intestinal flora plays a vital role in the pathophysiological processes of the body, and its quantity, diversity, and species proportion can all affect the body. Traditional Chinese medicines and natural products can regulate the richness and diversity of intestinal flora (Wenting et al., 2025) Lactobacillaceae, one of the bacterial families that has been most frequently associated with altered gut-brain interaction in PD (van der Maden et al., 2025). Our study shows that high myopia

https://doi.org/10.25135/rnp.2607.3975
Rec. Nat. Prod. 2027, 21(2):e26073975

causes anxiety via the Lactobacillaceae family of the gut microbiome, supporting the eye-brain-gut axis concept (Mi et al., 2024). The alleviating effects of a plant-based diet on inflammatory bowel disease, obesity, and type 2 diabetes are associated with an increased abundance of Muribaculaceae, a potential probiotic bacterial family (Zhu et al., 2024). Lachnospiraceae-mediated is associated with the colorectal tumorigenesis (Zong et al., 2025). Alloprevotella can be considered as a Potential Oral Biomarker in Intestinal Metaphase of Gastric Patients (Zong et al., 2025). Research has shown that the gut microbiota is closely associated with cancer development (Ordonez et al., 2025). As shown by the above results, the three drugs ZSG, HLS and BLJ all regulate intestinal flora to varying degrees and help restore intestinal flora to normal levels.

It is important to acknowledge the limitations of this study. First, the proposed mechanisms and compound-target interactions are primarily derived from molecular docking and network pharmacology computational predictions. Due to the limitations of rigid protein receptor docking, the results may not fully represent physiological binding behavior. Second, since absolute quantification was not performed, the relative contents provide semi-quantitative estimations rather than precise concentrations, which may limit detailed pharmacokinetic evaluation. Third, although the established pharyngitis animal model mimics the disease state, it cannot fully replicate the complexity of human clinical conditions, and the relatively small sample size may affect statistical power. Therefore, further experimental validation is essential to rigorously confirm the direct interactions and underlying biological mechanisms. Future studies will focus on addressing these gaps.

5 Conclusion

In summary, this study predicted the anti-pharyngitis mechanisms of ZSG, HLS and BLJ. The findings reveal that these medicinal plants exert their therapeutic effects via multi-component, multi-target, and multi-pathway. Key active compounds such as fisetin, alantolactone, kaempferol, artemisinin, and embelin interact strongly with core targets including SRC, TNF, PIK3CA, STAT3, and JAK2, primarily through pathways such as PI3K/AKT, Rap1, estrogen, and Ras signaling pathways, which collectively contribute to their anti-inflammatory and immunomodulatory actions. Furthermore, this study highlights the significant role of gut microbiota modulation in the therapeutic efficacy of these plants. All three species were found to regulate the composition and diversity of intestinal flora, particularly by restoring beneficial bacteria such as Muribaculaceae and Lachnospiraceae, thereby ameliorating microbial dysbiosis and supporting systemic immune homeostasis. These results not only deepen the understanding of the pharmacological basis of *Ardisia* species in treating pharyngitis but also provide a robust theoretical foundation for their further development into modern therapeutics.

Acknowledgement

This work was Supported by Guizhou Provincial Science and Technology Projects (Qiankehe foundation [2024] Youth 317), Zunyi City Science and Technology Innovation Team Construction (Zun KCTD (2025) 90); Zunyi City Technology Innovation Center (Zunshi Kehe CXZX [2025] 6); Zunyi Medical and Pharmaceutical College Team ([2026] 03), 2021 Academic New Seedling Training Project of Zunyi Medical University (Guizhou Science Platform Talents [2021]-036), Guizhou Administration of Traditional Chinese Medicine (QZYY-2025-020), Guizhou Key Laboratory of Modern Traditional Chinese Medicine Creation (Qian Ke He Platform ZSYS [2025] 019), Zunyi Medical University postdoctoral training fund project (ZYBSH[2024]016), Zunyi City science and technology plan project (ZunShiKehe HZ Zi (2024) 316), Innovation and entrepreneurship training program for college students (ZYDC202501154, S202510661735, ZYDC202501179).

Funding Statement

This work was Supported by Guizhou Provincial Science and Technology Projects (Qiankehe foundation [2024] Youth 317).

Author Contributions

Methodology: Zhonghui Nie, Xiaoshuang Wang, Ju Ye Software: Zhonghui Nie, Xiaoshuang Wang, Faming Wu, Sha Liu; Resource: Xiaoshuang Wang, Faming Wu, Sha Liu, Bo Huang, Ju Ye; Formal analysis: Zhonghui Nie, Chao Deng, Nana Tang, Xinyue Ke; Writing original draft: Zhonghui Nie; Writing review and editing: Xiaoshuang Wang, Ju Ye; Visualization: Zhonghui Nie; Project administration: Xiaoshuang Wang, Ju Ye.

Availability of Data and Materials

The authors declare that should any raw data files be needed about the further data of the study, they are available from the corresponding author upon reasonable request. Source data are provided with this paper.

Ethics Approval

All animal experiments were approved by the Laboratory Animal Ethics Committee of Zunyi Medical University (Approval No.: 56210202240601).

Artificial Intelligence (AI) Statement

The authors utilized Deepseek (2.6.1) for correcting grammatical errors. All content generated with the assistance of AI was thoroughly reviewed, verified, and sanctioned by the authors, who assume complete responsibility for the precision and integrity of the final manuscript.

Conflicts of Interest

The authors declare that they do not have any conflict of interest.

ORCID

Zhonghui Nie: 0009-0001-8967-7282
Sha Liu: 0000-0001-9781-1499
Faming Wu: 0009-0004-4284-3118
Chao Deng: 0009-0004-6269-6047
Nana Tang: 0009-0008-2234-3844
Xinyue Ke: 0009-0006-1673-4473
Bo Huang: 0009-0000-6971-5707
Xiaoshuang Wang: 0009-0005-9558-2449
Ju Ye: 0009-0007-8241-5865

References

An, J., Minie, M., Sasaki, T., Woodward, J. J. & Elkon, K. B. (2017). Antimalarial drugs as immune modulators: New mechanisms for old drugs. *Annual Review of Medicine*, *68*, 317–330. DOI: 10.1146/annurev-med-043015-123453.

Changzhi, Z. (2020). Observational study on the effect of Kaihoujian spray as adjuvant therapy in children with herpangina. *The Medical Forum*, *24*(2), 179–180. DOI: 10.19435/j.1672-1721.2020.02.019.

Cianciulli, A., Calvello, R., Porro, C., Trotta, T., Salvatore, R. & Panaro, M. A. (2016). PI3k/Akt signalling pathway plays a crucial role in the anti-inflammatory effects of curcumin in LPS-activated microglia. *International Immunopharmacology*, *36*, 282–290. DOI: 10.1016/j.intimp.2016.05.007.

Feifei, Z. & Jianlin, L. (2024). Efficacy and safety evaluation of kangfuxin liquid combined with Kaihoujian in the treatment of herpangina. *Heilongjiang Medicine Journal*, *37*(6), 1351–1353. DOI: 10.14035/j.cnki.hljyy.2024.06.037.

Fulin, Y., Yunhu, L., Yingquan, J., Xiongfei, C., Wei, W., Zhiwei, W., Jiangyong, A., Rendeqiang, Ning, D. & Shenghua, W. (2025). Response of yield and quality of radix Ardisia to soil physiochemical properties. *Acta Agriculturae Zhejiangensis*, *37*(8), 1766–1775. DOI: 10.3969/j.issn.1004-1524.20240630.

Hai, H., Rong, Z. X., Sha, Z. S., Yu, Z. X., Jia, C. Z. & Jing, S. (2022). Study on network pharmacology of fructus arctii-glycyrrhiza uralensispair against pharyngitis and establishment of HPLC methods forsimultaneous determination of 13 main active components. *Chinese Journal of Pharmaceutical Analysis*, *42*(9), 1522–1536. DOI: 10.16155/j.0254-1793.2022.09.05.

Heng, Z., Yufeng, W., Chunyu, T., Jianqiang, Z., Xionglong, W., Dan, L., Shiqi, L., Hongying, T., Shunxiang, L. & Wen, O. (2023). Exploring the mechanism of houyanqing in treating pharyngitis based on network pharmacology and experimental validation. *Modernization of Traditional Chinese Medicine and Materia Medica-World Science and Technology*, *25*(5), 1714–1728.

Hongbo, Y., Yongqiang, Z., Zhanggrong, L., Xin, W., Xin, Y. & Ying, Z. (2024). Chemical constituents from the roots of Ardisia crenata var. bicolor. *Chinese Pharmaceutical Journal*, *59*(4), 296–301. DOI: 10.11669/cpj.2024.04.002.

Hu, L., Zeng, Y., Ma, Y., Cao, H., Huang, C. & Zhang, L. (2027). Integrated phytochemical and network pharmacology revealing anti-photoaging, anti-inflammatory, and antioxidant activities of Tricholoma matsutake extracts. *Records of Natural Products*, *21*(1), e26033770. DOI: 10.25135/rnp.2603.3770.

Jin, W., Zhen, L., Hong, P. & Lei, L. (2025). Mechanism of jingyan pill in the treatment of chronic pharyngitis based onnetwork pharmacology analysis and molecular docking. *Chinese Journal of Otorhinolaryngology in Integrative Medicine*, *33*(1), 38–43. DOI: 10.16542/j.cnki.issn.1007-4856.2025.01.008.

Jin-He, Z., Hui, S., Ying, Z., Li-Yan, Z., Hai, Z., Xiu, D., Xiong-Wei, L. & Ting-Ting, F. (2022). Simultaneous determination of four constituents in Kaihoujian throat spray (for children) by QAMS. *Chinese Traditional Patent Medicine*, *44*(6), 1760–1765.

Linglian, K. & Zhigang, S (2026). Prediction on the mechanism of quercetin alleviating oxidative stress inbroilers based on network pharmacology and molecular docking. *China Poultry*, *48*(1), 45–52. DOI: 10.16372/j.issn.1004-6364.2026.01.006.

Liu, Y., Liu, Y., Zeng, C., Li, W., Ke, C. & Xu, S. (2022). Concentrated growth factor promotes wound healing potential of HaCaT cells by activating the RAS signaling pathway. *Frontiers in Bioscience*, *27*(12), 319. DOI: 10.31083/j.fbl2712319.

Liu, Y., Yin, Q., Liu, B., Lu, Z., Liu, M., Meng, L., He, C. & Chang, J. (2024). Fisetin reduces ovalbumin-triggered airway remodeling by preventing phenotypic switching of airway smooth muscle cells. *Respiratory Research*, *25*(1), 370. DOI: 10.1186/s12931-024-03005-8.

Lustofin, S., Kaminska, A., Bilinska, B., Wajda, J. & Hejmej, A. (2025). Role of estrogen signaling in notch pathway activation in sertoli cells. *Reproductive Sciences*, *32*, 2307–2318. DOI: 10.1007/s43032-025-01901-y.

Mi, Y., Chen, K., Lin, S., Tong, L., Zhou, J. & Wan, M. (2024). Lactobacillaceae-mediated eye-brain-gut axis regulates high myopia-related anxiety: From the perspective of predictive, preventive, and personalized medicine. *EPMA Journal*, *15*(4), 573–585. DOI: 10.1007/s13167-024-00387-z.

Min, D., Haining, Z., Qian, W. & Fang, H. (2024). Kaempferol suppresses inflammatory response and extracellular matrix damage in COPD model cells via inhibiting the PI3k/AKT signaling pathway. *Journal of Chinese Medicinal Materials*, *47*(8), 2063–2066. DOI: 10.13863/j.issn1001-4454.2024.08.032.

Oh, K. K., Adnan, M. & Cho, D. H. (2021). Network pharmacology study on morus alba l. Leaves: Pivotal functions of bioactives on RAS signaling pathway and its associated target proteins against gout. *International Journal of Molecular Sciences*, *22*(17), 9372. DOI: 10.3390/ijms22179372.

Ordonez, C., Zurita, S., Ramirez, G., Cordeiro, F., Garcia-Matamoros, K., Huaman-Garaicoa, F., Orellana-Manzano, A., Sandoya-Onofre, L., Pogo, J. & Carvajal-Aldaz, D. (2025). Are we there yet? Gut microbiota for cancer diagnosis, prognosis and treatment. *Seminars in Oncology*, *52*(4), 152376. DOI: 10.1016/j.seminoncol.2025.152376.

Peng, J., Liu, S., Liu, F., Qin, L., Wang, Q., He, Y., Zhang, D., He, W., Ke, X., Wu, F. & Wang, X. (2025). Substitutability evaluation and resource utilization of non-medicinal parts of Ardisia crenata Sims, a traditional ethnic medicine. *Physiologia Plantarum*, *177*(1), e70068. DOI: 10.1111/ppl.70068.

Qing, Y., Jin-Peng, C., Yue, L., Yi-Miao, L., Yi, L., Xiao-Hong, G., Cheng-Wang, T. & Chang-Qing, C. (2022). Research progress on chemical constituents and pharmacological effects of Ardisiae crenatae radix. *Chinese Traditional and Herbal Drugs*, *53*(9), 2851–2860.

Qunli, R., Qian, L., Huaqian, L., Faming, W., Yuqi, H., Jianguo, L. & Qian, W. (2024). Antitumor mechanism of Ardisia crenata radix. *Chinese Journal of Comparative Medicine*, *34*(1), 165–170.

Rui-Hang, H., Xin, Y., Yong-Qiang, Z., Chuan-Wen, L., Wei-Qian, Z. & Ying, Z. (2022). Chemical constituents from the roots of Ardisia crispa (thunb.) a. DC. *Chinese Pharmaceutical Journal*, *57*(8), 605–612.

Shihao, L., Xin, P., Zhiheng, W. & Zhiliang, G. (2024). Advances of research on pharmacological effects of fisetin. *Journal of Changshu Institute of Technology*, *38*(5), 47–53. DOI: 10.16101/j.cnki.cn32-1749/z.2024.05.006.

Sun, D., Yu, F., Ma, Y., Zhao, R., Chen, X., Zhu, J., Zhang, C., Chen, J. & Zhang, J. (2013). MicroRNA-31 activates the RAS pathway and functions as an oncogenic MicroRNA in human colorectal cancer by repressing RAS p21 GTPase activating protein 1 (RASA1). *Journal of Biological Chemistry*, *288*(13), 9508–9518. DOI: 10.1074/jbc.M112.367763.

van der Maden, M. M., Verbeek, M. M. & Beckers, M. (2025). Lactobacillaceae and Parkinson's disease: An apparent paradox. *Journal of Parkinsons Disease*, *15*(2), 269–281. DOI: 10.1177/1877718X241312401.

Wei, Q., Chang, L., Ying, Z., Qian-Qian, H., Yang, S., Zhao-Yan, D. & Xiong-Li, L. (2022). Mechanism of Ardisia crenata on rats with acute pharyngitis based on NF-κb/STAT signaling pathway. *Chinese Traditional and Herbal Drugs*, *53*(19), 6083–6092.

Weigang, W., Bin, F., Xiaolin, L., Shuibing, L., Xiaojuan, X., Ya, G. & Lining, H. (2025). Network pharmacology and molecular docking study on improving hypoxia tolerance of chebulae fructus. *Traditional Chinese Drug Research and Clinical Pharmacology*, *36*(1), 81–89. DOI: 10.19378/j.issn.1003-9783.2025.01.010.

Wenting, N., Shirong, L., Chenghong, S., Jingchun, Y. & Guimin, Z. (2025). Antithrombotic mechanism of jingfang mixture based on intestinal flora and metabolomics. *Chinese Traditional and Herbal Drugs*, *56*(7), 2396–2411.

Wenxi, W. & Jie, W. (2025). Effect of arctigenin on mucosal tissue damage in rats with chronic pharyngitis via modulation of the JAK2/STAT3 signaling pathway. *Chinese Journal of Gerontology*, *45*(9), 2230–2234.

Yang, D., Lin, J., Wang, T. & Liu, H. (2025). Advances in the regulation of gut microbiota metabolites by traditional Chinese medicine in the treatment of diseases. *Sheng Wu Gong Cheng Xue Bao*, *41*(6), 2236–2255. DOI: 10.13345/j.cjb.240996.

Yong, L., Wenming, S. & Wenxi, W. (2024). Influences of liyan syrup on pharyngeal tissue injury and pharyngeal mucosalrepair in rats with chronic pharyngitis based on JAK2/STAT3 signalingpathway. *Chinese Journal of Immunology*, *40*(1), 110–115.

Yuan, X., Li, J., Li, Y., Deng, Z., Zhou, L., Long, J., Tang, Y., Zuo, Z., Zhang, Y. & Xie, H. (2019). Artemisinin, a potential option to inhibit inflammation and angiogenesis in rosacea. *Biomedicine & Pharmacotherapy*, *117*, 109181. DOI: 10.1016/j.biopha.2019.109181.

Yun, F. (2021). Research progress on chemical constituents and pharmacological effects of inula helenium (elecampane). *Journal of Medicine & Pharmacy of Chinese Minorities*, *27*(12), 48–49. DOI: 10.16041/j.cnki.cn15-1175.2021.12.023.

Zaowei, Z., Guo, X., Qin, Y., Xinliang, M., Jiangang, Y., Xuting, W., Yulan, D. U. & Wenli, L. (2025). Exploring the mechanism of panax ginseng in relieving Sarcopenia based on network pharmacology and molecular docking. *Food and Fermentation Science & Technology*, *61*(2), 67–77.

Zhang, F., Sun, M., Ma, S., Sun, J., Li, Y., Li, X. & Jiang, H. (2025). Embelin mitigates the impact of perinatal inflammation on neuron development by inhibiting 5-lipoxygenase-mediated ferroptosis. *Phytotherapy Research: PTR*, *39*(9), 4060–4080. DOI: 10.1002/ptr.70052.

Zhang, H., Tong, Y., Jin, Y., Cai, G., Li, Z. & Pan, X. (2022). Elucidation of the mechanism of action of Runyan Mixture in the treatment of pharyngitis using a network pharmacological approach. *Medicine (Baltimore)*, *101*(51), e32437. DOI: 10.1097/MD.0000000000032437.

Zhao, Q., Wang, X., Jin, Y., Wu, T., Zhang, M., Shu, W., Li, H., Wen, J., He, Y., Chen, J., Chen, S., Liu, T., Zhang, J. & Liu, W. (2025). The effect of Yinhuang Hanhua dropping pill on acute pharyngitis via a systematic "compound-target-pathway" analysis. *Phytomedicine*, *139*, 156423. DOI: 10.1016/j.phymed.2025.156423.

Zhaoyan, D., Chang, L., Qianqian, H., Tingting, F., Wei, Q., Xiu, D. & Ying, Z. (2023). Mechanism of sophora tonkinensis in improving acute pharyngitis by regulating the leukocyte transendothelial migration pathway based on network pharmacology. *Chinese Pharmacological Bulletin*, *39*(2), 348–356.

Zhu, Y., Chen, B., Zhang, X., Akbar, M. T., Wu, T., Zhang, Y., Zhi, L. & Shen, Q. (2024). Exploration of the Muribaculaceae family in the gut microbiota: Diversity, metabolism, and function. *Nutrients*, *16*(16), 2660. DOI: 10.3390/nu16162660.

Zong, G., Deng, R., Pan, Y., Liu, M., Zhu, H., Tao, R., Shan, Y., Wei, Z. & Lu, Y. (2025). Ginseng polysaccharides ameliorate colorectal tumorigenesis through lachnospiraceae-mediated immune modulation. *International Journal of Biological Macromolecules*, *307*(Pt 2), 142015. DOI: 10.1016/j.ijbiomac.2025.14201.